Localization of Axonally Transported ^{125}I-Wheat Germ Agglutinin beneath the Plasma Membrane of Chick Retinal Ganglion Cells

JENNIFER H. LAVAIL,*‖ ILENE K. SUGINO,* and DONALD M. McDONALD*§
**Department of Anatomy, ‖Division of Neurobiology and §Cardiovascular Research Institute, University of California, San Francisco, California 94143*

ABSTRACT The distribution of ^{125}I-wheat germ agglutinin (WGA) transported by axons of chick retinal ganglion cells to layer *d* of the optic tectum was studied by electron microscopic autoradiography. We found that 52% of the radioactivity was located in axons and axon terminals in the contralateral optic tectum 22 h after intravitreal injection of affinity-purified ^{125}I-WGA. Axons comprised 43% of the volume of layer *d*. Dendrites, glial cells, and neuron cell bodies contained 20%, 17%, and 3% of the label, whereas these structures comprised 24%, 21%, and 2% of the tissue volume, respectively. We also measured the distances between the autoradiographic silver grains and the plasma membranes of these profiles, and compared observed distributions of grains to theoretical distributions computed for band-shaped sources at various distances from the plasma membranes. This analysis revealed that the radioactive source within axons was distributed in a band of cytoplasm extending in from the plasma membrane a distance of 63 nm. Because WGA is known to bind to specific membrane glycoconjugates, we infer that at least some glycoconjugates may be concentrated within an annular region of cytoplasm just beneath the axonal plasma membrane after axoplasmic transport from the neuron cell body.

In light of the specific affinity of wheat germ agglutinin (WGA) for *N*-acetylglucosamine and sialic acid, WGA has been widely used as a probe for membrane glycoconjugates containing these sugar groups (17, 49). For example, the binding of WGA to neuronal membranes has been used to study differences in the carbohydrate composition of neuron cell surfaces during development (14, 28, 34). We recently found that ^{125}I-WGA was selectively taken up by chick retinal ganglion cells and transported intact in their axons to the optic tectum (31). The rate at which the iodinated lectin was transported by these cells (30) was within the range of rates of anterograde transport of newly synthesized, endogenous proteins and glycoproteins (19, 24, 25).

The objective of the present study was to determine the location of the radio-labeled lectin within the tectum after anterograde axonal transport by chick retinal ganglion cells. To achieve this goal, we adapted the methods of analysis of electron microscopic autoradiography developed by Salpeter and others (see reference 56). We present evidence that (*a*) 52% of the radioactive label is found in axons and axon terminals; (*b*) the label within the axons is restricted to a narrow band of cytoplasm beneath the plasma membrane; and (*c*) nearly half of the radioactivity is present in dendrites and glia and therefore the lectin apparently is transferred from cell to cell after transport to the optic tectum.

MATERIALS AND METHODS

Preparation of Tissues: We used six 1- to 2-d-old cockerels (Feather Hill Farms Hatchery, Petaluma, CA). The WGA was iodinated then purified by affinity chromatography as previously described (31). Within 2 d of preparation, the ^{125}I-WGA (sp. act. 12–16 μCi/μg) was injected in 10–30 μl of 0.1 M phosphate buffer (pH 7.4) into the vitreal chamber of the right eye of each of five chicks anesthetized with diethyl ether. After 22–23 h the chicks were reanesthetized with choral hydrate (280 mg/kg body weight) and perfused through the heart with a mixture of glutaraldehyde and paraformaldehyde (22). Midbrains were removed, divided into right and left halves, rinsed several times with fresh fixative, and counted in a Beckman Biogamma counter with 70% efficiency (Beckman Instruments, Inc., Electronic Instruments Div., Schiller Parks, IL). Using a Vibratome (Oxford Laboratories, Inc., Foster City, CA), we cut 200-μm thick sections in the frontal plane from the optic tecta. Two or three sections of the caudal portion of the tectum were washed overnight in phosphate buffer (pH 7.4) with 5% sucrose. The following day the tissue was treated with reduced osmium (20), dehydrated, and embedded in Epon-Araldite. A sixth chick, which was not injected with ^{125}I-WGA, was anesthetized and perfused according to the same procedures and was

© The Rockefeller University Press · 0021-9525/83/02/0373/09 $1.00

used for the stereological analysis of cellular compartments in layer *d* of the optic tectum (see below).

Preparation of Autoradiographs: For light microscopic autoradiography, sections (1–2 μm in thickness) of the lateral convexity of the tecta were cut, mounted on glass slides, and coated with Kodak NTB2 or NTB3 emulsion (Eastman Kodak, Rochester, NY). The autoradiograms were developed 3, 5, or 8 wk after coating the sections.

For electron microscopy, sections 60–90 nm in thickness (51) were cut from two blocks from the lateral convexity of each caudoventral tectum. The sections were transferred to parlodion-coated glass slides, stained with lead citrate, and then coated with carbon. Half of the sections were coated with a monolayer of Ilford L4 emulsion (Polysciences, Inc., Warrington, PA) using the loop method of Salpeter and Bachmann (40). The other half were coated with the fine grain emulsion Kodak 129-01 (Eastman Kodak, Rochester, NY) (45). After 3–9 wk, sections coated with Ilford L4 emulsion were developed with Microdol X and those coated with Kodak 129-01 emulsion were developed with Dektol.

Sections were collected on 200-mesh copper grids and examined with the electron microscope to define the limits of layer *d* of the optic tectum (described below). While systematically scanning this layer at a magnification of 20,000, we photographed almost every silver grain visible in an area measuring ~60 × 400 μm. Prints from the negatives were prepared at a final magnification of 50,000.

Values for the resolution of each emulsion when used with ^{125}I were based on the integrated distribution of grains within 625 nm of a radioactive line source as described by Salpeter et al. (43). For a line source, one half-distance equals the distance from the source that includes 50% of the silver grains derived from that source. One half-distance for the Ilford L4 emulsion was ~90 nm; the half-distance for the Kodak 129-01 emulsion was found to be 60 nm. Background levels of radiation ranged from 0.003 to 0.005 grains/μm^2 for the Ilford L4 emulsion and from 0.003 to 0.025 grains/μm^2 for the Kodak 129-01 emulsion.

Stereological Analysis: In preparation for the "probability circle" analysis of autoradiograms (see below) we determined the proportion of layer *d* occupied by axons, dendrites, glia, neuron cell bodies, or vascular elements by photographing regions 11 μm^2 in area at equally spaced intervals across the thickness of the layer (total magnification = 50,000). The total area sampled was 134 μm^2. The cellular elements were analyzed using a coherent multipurpose test lattice (spacing = 15 mm) superimposed on the micrographs (55).

Autoradiographic Analysis: The distribution of silver grains in the autoradiographs was analyzed in two ways. The first involved a "probability circle" analysis (44). A circle with a radius equal to 153 nm for the Ilford emulsion coated sections and 102 nm for the Kodak 129-01 emulsion coated sections, i.e., equal to 1.7 half-distances (which contains 50% of the grains from a point source), was centered over each silver grain. Each grain was apportioned equally among the cellular elements (axons, dendrites, etc.) that the circle overlaid. The density of grains over each element was expressed as the ratio of the number of grains located over the element to the area occupied by that element.

A second analysis involved determining the position of the source of radiation in relation to the plasma membrane of axons, dendrites or glial cells. Specifically, our approach was to determine the number and density of autoradiographic grains at various distances from the plasma membrane of these structures. The observed frequency distributions were then compared with theoretical distributions computed for a line source or band-shaped sources of various widths and at various distances from the plasma membrane.

The distance from each silver grain to the plasma membrane (grain-distance) of the profile in question was measured on micrographs by using a digitizer (Talos Model 614B interfaced with a Hewlett-Packard Model 9815S computer). By using the grain distance measurements, each grain associated with a profile was attributed to one of 17 concentric annuli. The annuli were 0.5 half-distance wide and extended from a region 4.25 half-distances inside to a region 4.25 half-distances outside the plasma membrane. The distribution of grains on either side of the plasma membrane was obtained for all profiles by finding the total number of grains over each annulus (number of grains/annulus). For calculating grain densities, the perimeter (length of plasma membrane) of the profile being considered as the source for each grain was measured with the digitizer. From the perimeter and annulus width we computed the areas of the 17 concentric annuli. The mean grain density for each annulus was calculated by averaging the densities for that annulus from every profile (no. of grains/μm^2 of annulus). These mean values were used to generate the distribution of grain densities in the 17 annuli on both sides of the plasma membrane.

In calculating annular areas from perimeters, neuronal profiles were assumed to have a shape approximating circles, ellipses, or convex polygons. From theoretical considerations, infoldings (concavities) of the plasma membrane would result in calculated values being overestimates of actual annular areas. This effect would be most pronounced in the innermost annuli. To test how deviations from ideal geometric structures would affect our computations, we compared our computed values for annular areas with corresponding values obtained by measuring the concentric annuli directly with the digitizer. Three annuli from each of ten axons were measured. The differences in the average areas of the three annuli were +10.7% (outermost annulus), −4.5%, and 0% (innermost annulus), with an average difference of 2.1% (the average computed value being slightly larger than the average measured value).

Theoretical distributions for line sources and band sources were computed from equations similar to those of Salpeter et al. (41) (see Appendix). With a computer program, the optimal band-width (w), offset distance from the plasma membrane (l_0) and distance (δ) from the source were first estimated by a nonlinear least squares curve fitting procedure. The program repeatedly tested different band-widths, offsets, and distances until the theoretical distribution most closely fit the observed distribution. From this initial test, we found the best-fitting curve described a source immediately adjacent to the plasma membrane. In subsequent tests, we only estimated the band width and distance from the source.

The significance of differences in the observed and predicted distributions of silver grains was assessed by using the Kolmogorov-Smirnov test (50). In this test the P value is calculated from the number of values and the maximal difference (D_{max}) in cumulative frequency distributions.

For the second kind of analysis, only sections coated with Kodak 129-01 emulsion were used because of its better resolution. We analyzed separately those axons containing four or more synaptic vesicles (axon terminals; n = 201) and those that contained fewer than four synaptic vesicles (axons; n = 161). The problems due to radiation from adjacent sources were minimized by including for analysis only those grains that satisfied three criteria: first, they had a silver grain lying within 300 nm (i.e., five half-distances) of the plasma membrane of a given type of profile; second, they were located >300 nm from the plasma membrane of another similar profile; and third, the reference plasma membrane was cut in cross-section. Only about one-third of the silver grains positioned over axons met these criteria.

To assure ourselves that the band-shaped distribution of radioactivity we found was not somehow the result of the exclusion of silver grains located within five half-distances of two potential sources, we chose 57 other silver grains that were not analyzed earlier because they were located near two possible axonal sources. We measured the distance from the center of each grain to the nearest axonal plasma membrane. 57% of the silver grains were found to lie within an axon. As in the case of the 362 silver grains used for the main hypothetical source analysis, they were most concentrated in the region of axoplasm within 60 nm of the plasma membrane.

RESULTS

Morphological Observations

Layer *d*, situated in the outer one-third of the optic tectum, is ~60 μm in thickness and contains few neuronal cell bodies (21, 36). This scarcity of neuronal cell bodies provides the most useful criterion by which to define the boundaries of layer *d* in thin sections; adjacent laminae contain many more neurons. Myelinated fibers are rare, because only ~5% of the optic nerve fibers are myelinated in chicks of this age (35).

Radially oriented axons, <0.75 μm in diameter, extend from the stratum opticum at the surface of the tectum through the intervening layers to layer *d* (21). From the stereological analysis we found that ~18% of layer *d* was occupied by profiles that we considered to be axons, based on their characteristic regular array of microtubules, absence of ribosomes, regular contour and content of less than four synaptic vesicles (Fig. 1). Another 25% of the area was filled with axonal profiles that contained at least four vesicles ~50 nm in diameter (Fig. 3). In some cases a presynaptic density was also present. The latter were considered to be axon terminals as most of them closely resembled the synaptic terminals described previously in studies of this layer of the tectum in pigeons (2, 15).

The dendrites (which may be up to ~1.2 μm in diameter) of piriform neurons located in deeper layers extend into layer *d*. There are also larger, circumferentially directed dendrites of stellate neurons whose cell bodies are located within the layer (13). From the stereological analysis we found that dendritic profiles occupied ~24% of the area of layer *d*. Most of these had an irregular shape, contained ribosomes and a comparatively lucent cytoplasm and were postsynaptic to other elements (Fig. 5). We also included in the category of dendrites, unmye-

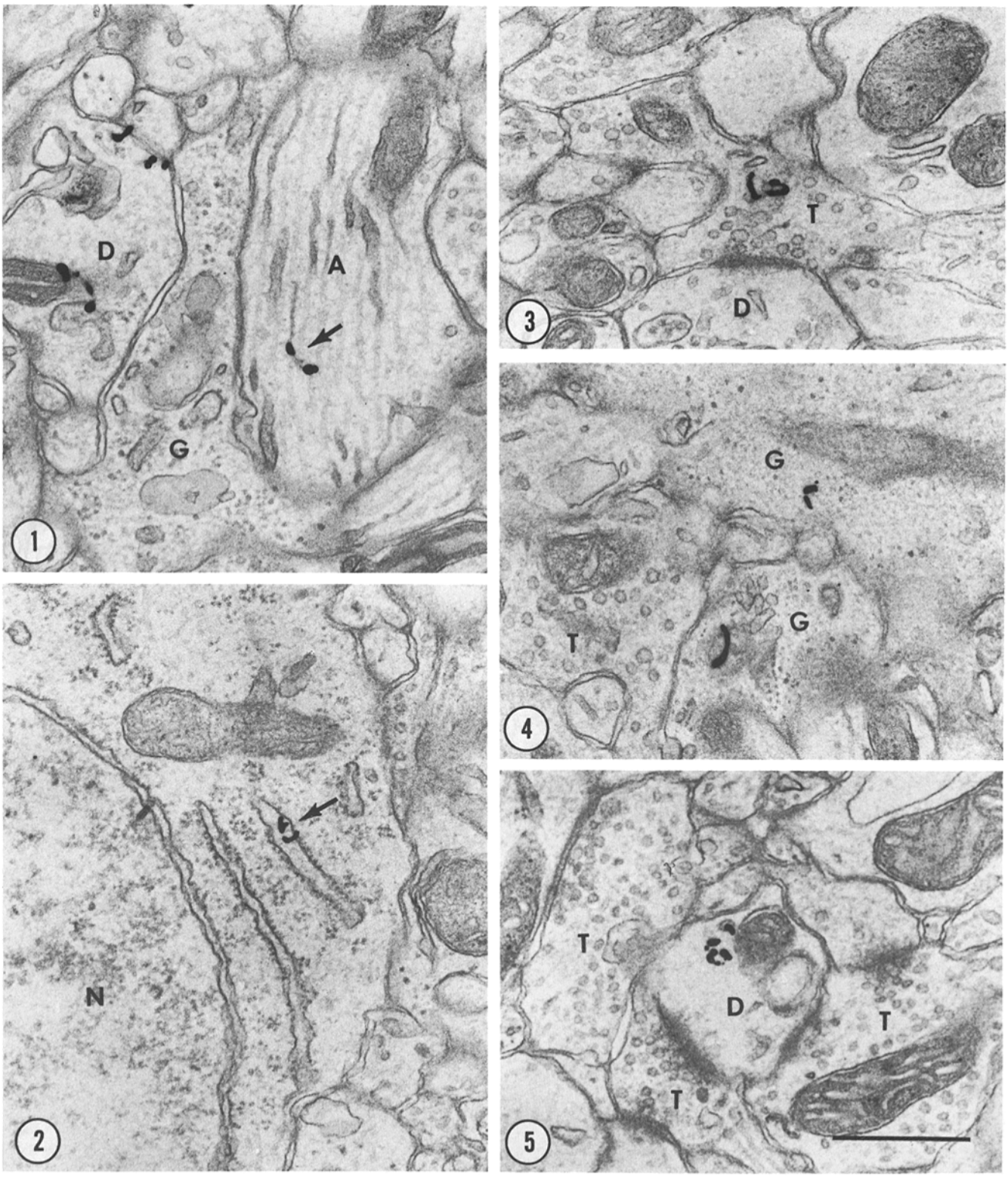

FIGURES 1–5 Electron microscopic autoradiograms from layer *d* of the chick optic tectum 22–23 h after an injection of ^{125}I-WGA into the vitreal chamber of the contralateral eye. All of the sections illustrated were coated with Kodak 129-01 emulsion. Fig. 1: A labeled (arrow) axon profile containing several cisternae of smooth endoplasmic reticulum and numerous microtubules. Other silver grains are located over a nearby dendritic profile. Fig. 2: A portion of a labeled (arrow) neuron cell body. Fig. 3: A labeled axon terminal which contains numerous synaptic vesicles that is presynaptic to a dendrite. Fig. 4: Labeled glial cell processes near an axon terminal. Fig. 5: A labeled dendritic profile adjacent to several axon terminals. *A*, Axon. *D*, Dendrite. *G*, Glia. *N*, Nucleus. *T*, Axon terminal. Bar, 0.50 μm. × 48,000.

linated profiles that were >0.75 μm in diameter and contained a regular array of microtubules. Some of these profiles contained a cluster of small vesicles near the plasma membrane, and thus may be presynaptic dendrites. Our assumption that these profiles were dendrites was based on their resemblance to the horizontal or circumferential dendrites described by

Hayes and Webster (15) and on the observation that they failed to disappear from layer *d* after eye removal in young chicks (T. P. Margolis and J. LaVail, unpublished observations).

Probability Circle Analysis

In the chick all axons of retinal ganglion cells cross in the optic chiasm and end in the opposite side of the brain. Thus, the radioactivity on the ipsilateral side of the brain can be used as a measure of radioactivity not due to axonal transport. In the contralateral optic tectum, radioactivity due to axoplasmic transport (defined as disintegrations per minute (dpm) in the contralateral minus dpm in the ipsilateral tectum) consisted of an average of 9,348 ± 3,786 dpm (SD; $n = 5$).

The probability circle analysis of the autoradiograms revealed that axons had the highest grain density (0.124 grain/μm^2). (Fig. 1, Table I) We found axon terminals (Fig. 3) had a grain density of 0.083 grains/μm^2. We also observed that the radioactivity was concentrated over neuron cell bodies, dendrites and glial cells. The few neuron cell bodies that we found in layer *d* contained a concentration of grains almost as great as axons (Fig. 2). The density of labeling over dendrites (Fig. 5) and glial cells (Fig. 4) was about half that over axonal profiles (Table I). Blood vessels, including the vessel wall and lumen, had a labeling density of 0.014 grain/μm^2 (near background). The category designated "other" included those profiles which we could not define as axonal or dendritic. This compartment (presumed to be mainly axons and dendrites) had a high density of labeling (Table I). The distribution of label among the various elements was significantly different than random as determined by Chi-square analysis ($P < 0.001$; 5 degrees of freedom [df]).

Analysis of Intraaxonal Distribution of Radioactivity

Because casual observations suggested to us that silver grains were most numerous near the surface of axons, we used the plasma membrane as a reference and calculated the concentration of silver grains at various distances from this membrane.

The first population examined included all axons (both axons and axon terminals). Silver grains were distributed asymmetrically about the plasma membrane of axonal profiles. Of all grains within 4.25 half-distances of the axolemma, 64% were positioned over structures located inside the axons (Fig. 6). However, silver grains were not uniformly distributed over the axoplasm. Instead they tended to be concentrated near the plasma membrane. The observed distribution of grains had a broad peak (Fig. 6) and thereby did not fit the theoretical distribution for a line-source of radiation, as would be expected if the plasma membrane was the sole site of the label (D_{max} = 27.6%, $P < 0.001$). Furthermore, the observed distribution was centered inside the plasma membrane rather than over it. The data fit best a band-shaped source of radiation that extended in 63 ± 10 nm from the plasma membrane (Fig. 7).

To evaluate this population of axons further, we analyzed separately axons and axon terminals (Fig. 8). In both groups the silver grains were concentrated inside the axonal membrane. Although axon terminals had a 33% lower grain density than did axons themselves, the differences in the distributions of grains in the two groups of axons was not significant (D_{max} 15.7%, $P > 0.5$).

The distribution of silver grains over axon terminals fit best a band-shaped source 62 ± 16 nm that extended inward from the axolemma (Fig. 9). In the case of axons, the band was 62 ± 12 nm wide (Fig. 10).

In dendrites the highest grain density also was located inside the plasma membrane, but the distribution formed a broad plateau instead of a sharp peak as found for axons (Fig. 11). This plateau of labeling was also seen in the population of glial profiles (Fig. 6). Only 35% of the silver grains were located inside the plasmalemma of glial profiles. Most silver grains

TABLE I

*Grain Densities of Cellular Elements in Layer d of Chick Optic Tectum Based on Probability Circle Analysis**

Compartment	No. of grains (% of total)	Area (μm^2)§ (% of total)	Grain density (grains/μm^2)
Axons	281 (27.0)	2,263 (18)	0.124
Axon terminals	261 (25.1)	3,143 (25)	0.083
Dendrites	212 (20.4)	3,018 (24)	0.070
Glia	178 (17.1)	2,640 (21)	0.067
Neuronal cell bodies	30 (2.9)	251 (2)	0.120
Blood vessels	9 (0.9)	629 (5)	0.014
Other	69 (6.6)	629 (5)	0.110
Total	1,040 (100.0)	12,573 (100)	0.083

* Because significant differences were not found by analysis of variance when grain densities for different animals were compared (obtained from sections coated with the same emulson), the results of animals were combined. The differences in densities obtained with different emulsions were also not significant by an analysis of variance when differences in emulsion sensitivity were considered (8, 42). In our case, the Kodak 129-01 emulsion was 71% as sensitive as the Ilford emulsion.

§ The areas were measured by point-counting (see Materials and Methods). The percent of the total was calculated by multiplying the area of each micrograph (16 × 42 μm^2) by the number of micrographs and the proportion of the total area occupied by the element.

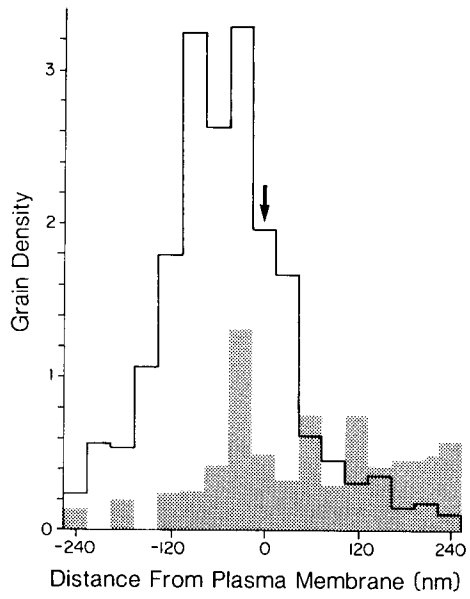

FIGURE 6 Histograms showing the density of silver grains (no. of grains per μm^2 of cytoplasm) over all axons and axon terminals (solid line) and over glial profiles (stippled) at various distances from their respective plasma membranes (designated by 0 and the arrow; negative numbers are inside the profile). The histograms are based on grains over 362 axonal profiles (average diameter of 1.0 μm) and 139 glial profiles (average diameter of 0.8 μm).

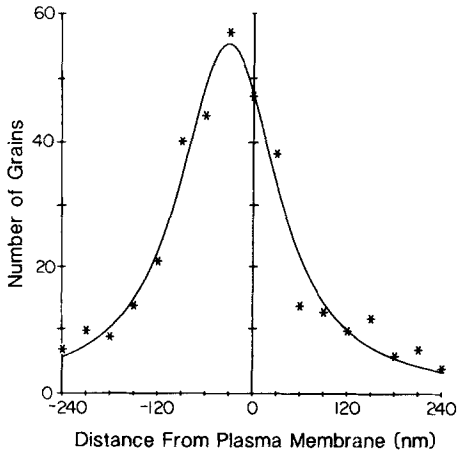

FIGURE 7 Asterisks indicate the number of silver grains present over 362 axons and axon terminals at various distances inside (negative numbers) or outside their plasma membrane. The curve describes the theoretical distribution of grains about a band-shaped source that has a width of 63 ± 10 nm and extends in from the plasma membrane. This particular curve provides the best fit for the observed values by a nonlinear method of least squares.

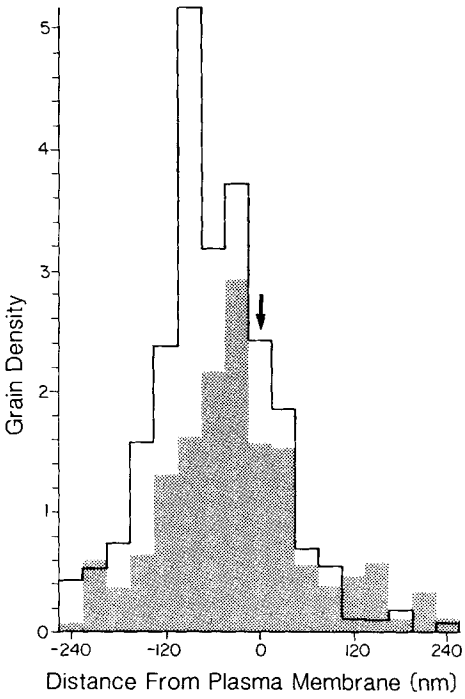

FIGURE 8 Histograms showing the density of silver grains (no. of grains per μm^2 of cytoplasm) over axons (solid line) and axon terminals (stippled) at various distances from the plasma membrane (designated by 0 and the arrow). The histograms are based on grains over 161 axon profiles (average diameter of 1.0 μm) and 201 axon terminals (average diameter of 0.9 μm).

outside the plasma membrane of glia appeared to overlie nearby axonal profiles. In addition, there was a small peak of labeling located ~60 nm inside the membrane of the glial cells. The grain density distributions for glia and dendrites were significantly different from each other (D_{max} = 44.0%; $P < 0.001$) and also were different from axonal profiles (D_{max} = 40.1%; $P < 0.001$ for glia and D_{max} = 30.2%; $P < 0.001$ for dendrites).

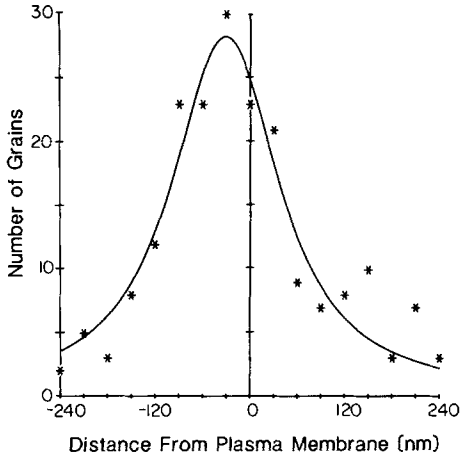

FIGURE 9 Asterisks indicate the number of silver grains located at various distances inside and outside the plasma membrane of 201 axon terminals. The curve describes the theoretical distribution of grains about a band-shaped source that is 62 ± 16 nm wide. The particular curve provides the best fit for the observed values by a nonlinear method of least squares.

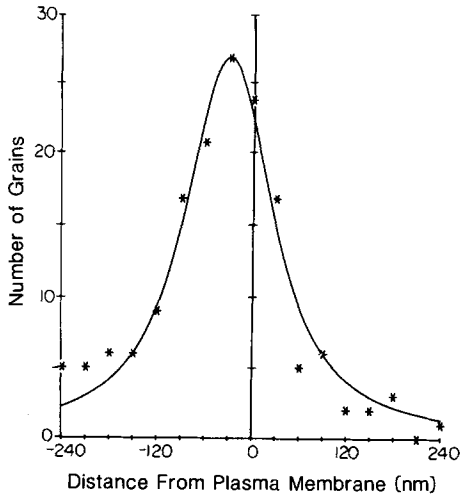

FIGURE 10 Asterisks mark the number of silver grains located over axons (n = 161), as plotted in Fig. 9. The curve describes the theoretical distribution of grains about a band-shaped source that extends in from the plasma membrane a distance of 62 ± 12 nm.

DISCUSSION

Axonal Labeling

On the basis of the results of the probability circle analysis and the concentration of silver grains over axonal profiles, we conclude that the iodinated WGA is transported by retinal axons to their endings in layer *d* of the optic tectum. This process occurs in <22 h after intravitreal injection. Axons (excluding their terminals) occupy only 18% of the total area of sections of layer *d*, but they are the source of 27% of the silver grains (Table I). On the average, axons have about twice the radioactivity of dendrites or glial cells and nine times that of endothelial cells. The observation of silver grains over neuronal cell bodies and glial cells led us to suspect that our radioactive probe was not strictly confined to retinal ganglion cell axons (see below). Therefore, some labeled profiles probably were portions of second-order neurons.

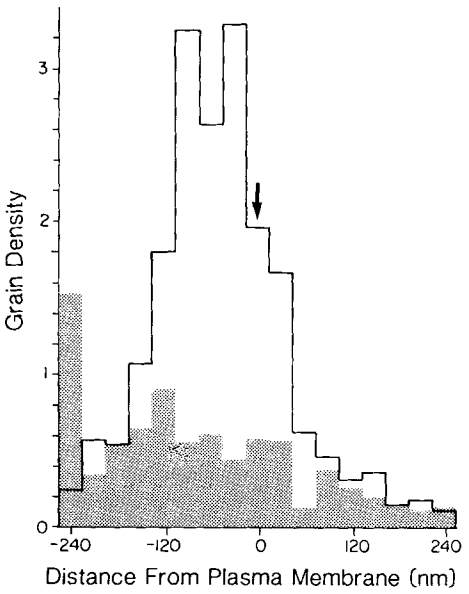

FIGURE 11 Histograms showing the density of silver grains (no. of grains per μm^2 of cytoplasm) over all axon and axon terminal profiles (solid line) repeated from Fig. 6 for comparison with the density of silver grains over dendritic profiles (stippled). The dendritic histogram is based on grains over 153 profiles (average diameter of 0.8 μm).

Intraaxonal Distribution

Within axonal profiles the radioactive lectin did not appear to be restricted to the plasma membrane. Instead it was concentrated in a 63 nm wide band just beneath the plasma membrane. The band appeared to be approximately the same width in axons as in axon terminals.

The actual width of the band is probably narrower than 60 nm because our model for analyzing grain distributions did not consider the plane of section in which the zone of radioactivity was cut in different axons. In our material axons had an average aspect ratio (eccentricity) of four. From this value we infer that axons were cut in planes averaging 75° from cross-section. Assuming that axons are cylindrical and the zone of radioactivity is a uniformly thick layer beneath the plasma membrane, then the apparent width of the zone in axons cut at 75° would be as much as fourfold the actual width (a function of the secant of 75°). Thus, the actual width (44 nm) would be 27% less than the average apparent width (60 nm).

Radioactivity in the vicinity of the axolemma has been reported by several groups of investigators who have used a variety of neurons and radioactive probes to trace the fate of newly synthesized proteins and glycoconjugates in axonal transport (3, 5, 7, 11, 16, 23, 47, 52). Our results with an exogenously applied and incorporated lectin most clearly resemble those of Lentz (23) who used [^{3}H]leucine as a precursor for axonally transported newly synthesized protein in regenerating brachial nerves of the newt. In his study the experimental distribution of grains most closely fit a source shaped as a solidly labeled circular band with an inner radius of 600 nm and an outer radius of 1,350 nm located 150 nm inside the axolemma. He found no evidence that the axolemma was a major site of accumulation of radioactive molecules.

However, the fact that Lentz used tritiated leucine and regenerating nerves complicates further comparison of his work with ours. For example, probes such as leucine or fucose that are incorporated into a wide spectrum of glycoconjugates result not only in higher specific activities but also in a more uniform distribution after axonal transport. Furthermore, we chose to use ^{125}I as the isotope and the Kodak 129-01 as the emulsion for this level of analysis because these provided us with twice the resolution achieved with other commonly used isotopes and emulsions (43).

Recently, Lasek et al. (54) have proposed that endogenous proteins are transported in the axon as components of intact cytological structures. Among the organelles that have been implicated in the role of transporting endogenous proteins at a rapid rate are: the axolemma (29), mitochondria (9, 27), vesicles (53), and smooth endoplasmic reticulum (7, 47). Since WGA is rapidly transported in axons of retinal ganglion cells, could the transport of the lectin be associated with one of these organelles? Alternatively, might any of these organelles be a site of accumulation of ^{125}I-WGA after transport?

Because the peak of labeling in our study does not coincide with the plasma membrane, it seems unlikely to be the principal source. Moreover, neither mitochondria nor clustered synaptic vesicles in axon terminals appear to have a distribution that coincides with the distribution of silver grains.

Elements of the smooth endoplasmic reticulum and vesicular organelles, however, cannot be excluded as sources. Elements of the smooth endoplasmic reticulum, called the hypolemmal cistern (33, 37), are commonly observed in this region, and small vesicular and tubular profiles do occur infrequently near the axon membrane (Fig. 1). The precise distinction between hypolemmal cisterns and small vesicles remains unclear. Schnapp and Reese (46) have studied turtle optic nerves with the techniques of rapid-freezing and cryoprocessing in order to examine the cytoplasmic structure of the axon. They found elements of the smooth endoplasmic reticulum in a distinct zone up to 100 nm wide next to the axonal plasma membrane.

Furthermore, Wood et al. (57) have proposed that complex oligosaccharides are present in hypolemmal cisterns of Purkinje cell axons. They used peroxidase conjugates with WGA or concanavalin A to characterize carbohydrates of neuronal membranes in fixed sections of chick cerebellum. Although they found labeling of the plasma membrane and hypolemmal cisterns with concanavalin A, complex sugars in the hypolemmal cisterns apparently failed to bind the WGA conjugated with horseradish peroxidase. Whether axons of chick retinal ganglion cells contain elements of smooth endoplasmic reticulum in this location throughout the axon and whether these elements would bind WGA remain to be determined. However, if so, the hypolemmal cisterns would be strong candidates for binding of transported WGA.

The localization of most of the transported lectin free in the cytoplasm appears unlikely for several reasons. First, results of subcellular fractionation indicate that >80% of the radioactivity recovered from the optic tectum after transport by chick retinal ganglion cells is associated with membranes (T. P. Margolis and J. LaVail, manuscript in preparation). Second, the rate of transport of ^{125}I-WGA (22–44 mm/d) (30) corresponds to the rate at which endogenous glycoproteins are transported (19, 24), and these are presumably membrane-associated proteins. Lastly, assuming that the ^{125}I-WGA is taken up by the retinal ganglion cells by endocytosis (12), the lectin would have to cross a membrane to escape into the cytosol.

Intercellular Transfer of Radioactivity

The presence of ^{125}I-WGA in neuron cell bodies, dendrites,

and glial profiles in the tectum was suggested by the results of the probability circle analysis and further supported by data from the hypothetical source analysis. The possibility that WGA could be transferred from autonomic ganglion cells to preganglionic terminals after retrograde axonal transport was discounted by Schwab et al. (48), who examined the labeling in the superior cervical ganglion after retrograde axonal transport following eye injections of WGA conjugated to horseradish peroxidase. Ruda and Coulter (38), however, did raise the possibility of intercellular transfer of WGA after anterograde transport based on their immunocytochemical identification of the lectin in neuronal perikarya of the rat superior colliculus after vitreal injection of WGA. Assuming that the iodine label we find over cell bodies, dendrites, and glial processes is neither iodinated tyrosine fixed in these cells by glutaraldehyde nor tyrosine reincorporated into protein, then our results support the hypothesis of intercellular transfer of the lectin after its anterograde axonal transport. It is unknown how the lectin would be taken up by the ganglion cells but not degraded, or by what mechanisms it leaves the first neuron and then is incorporated by a second cell.

Possible Intracellular Pathways

Questions about how the WGA is taken into the retinal ganglion cell, how it is processed within the cell body and transferred into the axon remain to be investigated. The initial step of uptake is assumed to depend on the selective binding of the WGA to surface glycoconjugates. Evidence that horseradish peroxidase conjugated to WGA is taken up by adsorptive endocytosis (12) suggests that the iodinated lectin is processed in the same way. This assumption is further supported by the fact that the uptake of the iodinated, affinity-purified WGA appears to be specific, since WGA that has lost its affinity for *N*-acetylglucosamine is not taken up and transported by the ganglion cells (31).

Once WGA is taken into the cell, one could envisage several intracellular paths. WGA could remain associated with endocytosed components of the plasma membrane, as has been suggested for epidermal growth factor iodinated with chloramine-T (6), in which case some of the endocytosed vesicular membrane might avoid fusion with other membranous systems. If this hypothetical pathway were to exist, then the intracellular location of the ^{125}I-WGA within the axon, as shown in the present study, would reflect a novel path followed by perikaryal plasma membrane. Alternatively, endocytosed lectin might follow a path similar to that described by Abrahamson and Rodewald (1) in which vesicular organelles mediate the transfer and release of intact IgG across the intestinal epithelial cell without involvement of the components of the Golgi complex region. Consistent with this model is our finding of the apparent release of ^{125}I-WGA from retinal ganglion cell axons in the optic tectum.

Another and possible parallel path involves the fusion of endocytotic vesicles containing the lectin with lysosomal organelles. In this regard, Harper et al. (12) have found that the lysosomal system, including a region of the Golgi system that contains acid phosphatase activity, contains the conjugated lectin after its introduction into the vitreous of the rat eye. This suggests that we might also find the affinity-purified lectin in this compartment of the cell body. The transfer of the lectin to elements of the Golgi system and lysosomes resembles that taken by other specifically endocytosed molecules, such as horseradish peroxidase conjugated to epidermal growth factor (56). It is tempting to speculate that it is at this point that the intact lectin would be transferred to smooth vesicular organelles that under some conditions have been found to be involved in the anterograde transport system of the axon (4). How the lectin would be protected from degradation in these organelles remains to be explored.

Based on similarities in rate of transport (9, 18, 19, 24, 30) and location within the axon (5, 7, 23) after transport of exogenously applied WGA and endogenously synthesized proteins, the transport of the lectin hypothetically could also be involved with the transport of newly synthesized glycoconjugates (10, 24, 32, 39). After processing in the Golgi system, the lectin would travel with membranes destined for secretion with neurotransmitter or delivery to the cell surface. If the intracellular path of the WGA did reflect the path of newly synthesized proteins, then it might serve as a useful probe for the study of proteins moving with it. The proteins moving at ~40 mm/d (Group II) (27) remain largely unexplored except for fodrin, two polypeptides that are also located beneath the plasma membrane of many cell types (26). However, with any of these intracellular paths the possibility remains that the binding of the lectin to the ganglion cell surface has modified the process of normal endocytosis and subsequent membrane movement through the cell.

APPENDIX: DERIVATION OF THE FUNCTIONS DESCRIBING A PROJECTION ONTO A PLANE OVER A BAND-SHAPED SOURCE [1]

We derived the functions for the distribution of grain densities in a plane overlying a point source, f_p, a line source, f_l, and a band source, f_b, of radiation.

Consider a point source S that is positioned a distance δ from the plane and emits particles isotropically (Fig. 12). The fraction of the particles that reaches the plane within a circle whose radius is ζ is the ratio of the surface area of the polar cap to total surface area of the hemisphere. Given the distance δ, the radius ζ of the polar cap determines the radius ρ of the hemisphere. Because the surface area of the polar cap is $2\pi\rho\,(\rho - \delta)$ and the surface of the hemisphere is $2\pi\rho^2$, and because $\rho^2 = \zeta^2 + \delta^2$, the fraction of the particles reaching the plane within the circle of radius ζ is:

$$F_p = \frac{2\pi\rho\,(\rho - \delta)}{2\pi\rho^2} = \frac{\rho - \delta}{\rho} = 1 - \frac{1}{\sqrt{1 + (\zeta/\delta)^2}} \qquad (1)$$

Assuming complete absorption of the energy, the grain density, f_p, i.e., the number of grains per unit area, is proportional to the fraction of the particles that hit the plane within an annulus of radius ζ and width $d\zeta$ (Fig. 12) divided by the area of the annulus:

$$f_p(\zeta) \sim \frac{dF_p}{2\pi\zeta d\zeta} \sim \frac{1}{\sqrt{(\delta^2 + \zeta^2)^3}} \qquad (2)$$

Eq. 2 describes the grain density due to a point source at a distance ζ away from the normal projection of the point on the plane separated by a distance δ from the point source. This equation is identical to Eq. 5 in the appendix of Salpeter et al. (41), except for the scaling factor and notation, i.e., $\delta \equiv d$; $\zeta \equiv x$.

For a radioactive source distributed homogeneously along a line, a given point 0 on the plane has a grain density that receives a contribution of the above magnitude from every point source along the line. The grain density, f_p, expressed in terms of p, a normal projection of the distance ζ on the line (Figs. 12 and 13), can be expressed as follows, considering that $\zeta^2 = q^2 + p^2$:

$$f_p \sim \frac{1}{\sqrt{(\delta^2 + q^2 + p^2)^3}} \qquad (3)$$

Thus, the total grain density (f_l) is the sum of all contributions from the points located a distance p away from the normal projections of point 0 on the line:

[1] Prepared by Vojtech Ličko, Donald M. McDonald, and Jennifer H. LaVail. V. Ličko is a member of the Cardiovascular Research Institute, University of California, San Francisco.

$$f_l(q) = \int_{-\infty}^{\infty} f_p(p)dp = \frac{1}{2(\delta^2 + q^2)} \int_{-\infty}^{\infty} \frac{dv}{v^{3/2}} \sim \frac{1}{\delta^2 + q^2}. \quad (4)$$

The above integral was solved by using the substitution:

$$\frac{\delta^2 + q^2}{p^2} + 1 = v. \quad (5)$$

For a homogeneous source located in a band oriented parallel to the plane, the grain density is the sum of the contributions of all points in the band (Fig. 14). Every point in the band contributes by:

$$f_p(p, z) \sim \frac{1}{\sqrt{[\delta^2 + (q_0 + z)^2 + p^2]^3}}, \quad (6)$$

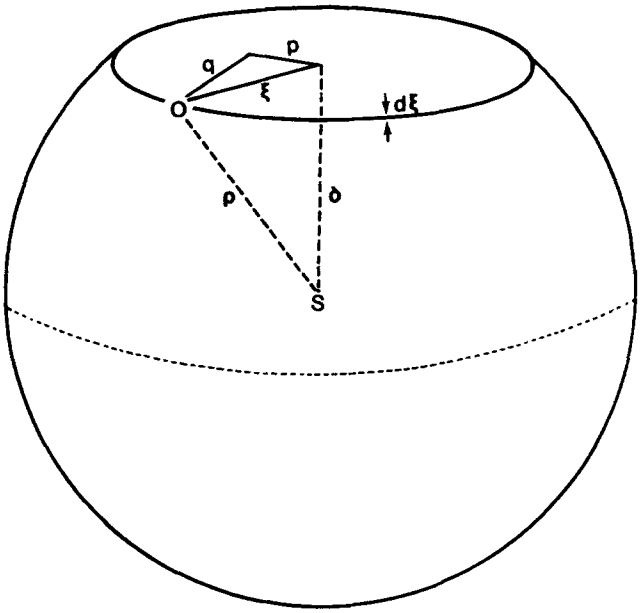

FIGURE 12 Diagram to illustrate the geometry of a plane overlying a point source. The polar cap created by the section of the sphere by the plane has been removed. In the figure δ is the distance of the plane from the point source, S; ζ is the distance between the point of observation 0 and the normal projection of the point source onto the plane; ρ is the radius of the sphere. The figure also illustrates a variable point source on a portion of a line that is projected onto the plane as p. Thus, q indicates the distance of the point 0 normal to the line p. Eq. 2 describes the grain density as a function of ζ, i.e., at a variable point of observation 0 in the plane at a distance δ away from the point source S. Eq. 4 describes the grain density at 0 as a function of q, i.e., at a variable distance q from the line p.

where q_0 is the distance from the point of observation to the edge of the band and $q = q_0 + x$ (Fig. 14).

The grain density distribution for a band source, f_b, then is:

$$f_b(l) = \int_{l_0}^{l_0+w} \int_{-\infty}^{\infty} f_p(p, z)\, dpdz \sim \arctan\frac{2l_0 - l + w}{\delta} - \arctan\frac{2l_0 - l}{\delta}, \quad (7)$$

where l_0 is the distance from an arbitrarily chosen point of reference M to the edge of the band and l is the distance from M to 0.

A nonlinear least-squares procedure was used to estimate the parameters $1/\delta$, w/δ, and $2l_0/\delta$, so that δ, the distance of the band source from the plane, w, the band width, and l_0, the distance of the band from the reference point, could be estimated.

The authors are grateful to Todd P. Margolis for his contribution of the affinity-purified ^{125}I-WGA, to Diane D. Ralston for help with the electron microscopic autoradiography, to Amy Haskell and Earl McDonald for their assistance with the computer programs, and to Mary Helen Briscoe for assistance with the illustrations. We also thank Alana Schilling for secretarial help.

The work was supported in part by National Institutes of Health PHS R01 NS 13533 and Program Project grant HL 24136.

Received for publication 29 June 1982, and in revised form 25 October 1982.

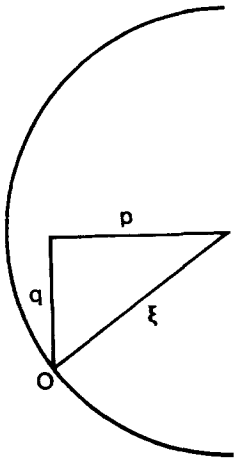

FIGURE 13 Diagram to illustrate the plane overlying a portion of a line source of radiation projected onto the plane as p.

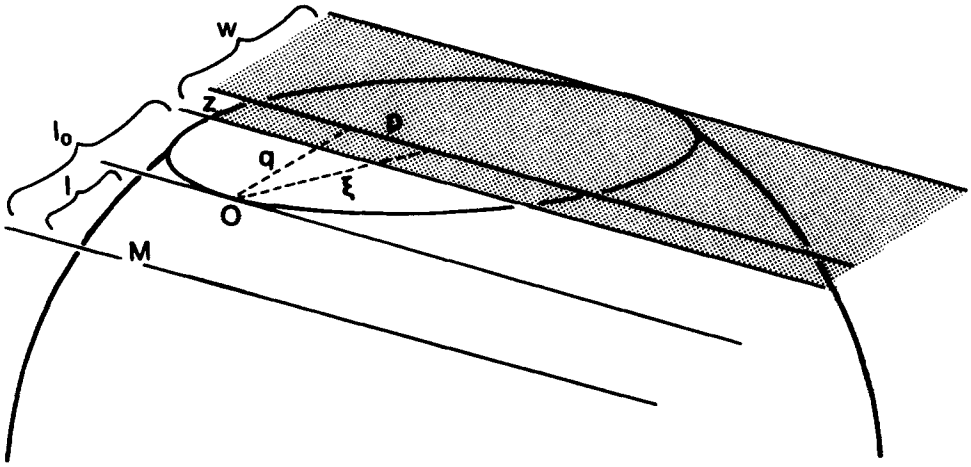

FIGURE 14 Diagram to illustrate the relationship of a band-shaped source of width (w) projected onto the plane and the off-set of the band, l_0 from a reference point M projected from the plane of the source onto the overlying plane.

REFERENCES

1. Abrahamson, D. R., and R. Rodewald. 1981. Evidence for the sorting of endocytic vesicle contents during receptor-mediated transport of IgG across the newborn rat intestine. *J. Cell Biol.* 91:270–280.
2. Angaut, P., and J. Reperant. 1976. Fine structure of the optic fiber termination layers in the pigeon optic tectum: a Golgi and electron microscope study. *Neuroscience.* 1:93–105.
3. Bennett, G., L. di Giamberardino, H. L. Koenig, and B. Droz. 1973. Axonal migration of protein and glycoprotein to nerve endings. II. Radioautographic analysis of the renewal of glycoproteins in nerve endings of chicken ciliary ganglion after intracerebral injection of [^{3}H]fucose and [^{3}H]glucosamine. *Brain Res.* 60:129–146.
4. Broadwell, R. D., C. Oliver, and M. W. Brightman. 1980. Neuronal transport of acid hydrolases and peroxidases within the lysosomal system of organelles. Involvement of agranular reticulum-like cisterns. *J. Comp. Neurol.* 190:519–532.
5. Byers, M. R. 1974. Structural correlates of rapid axonal transport: evidence that microtubules may not be directly involved. *Brain. Res.* 75:97–113.
6. Comens, P. G., R. L. Simmer, and J. B. Baker. 1982. Direct linkage of ^{125}I-EGF to cell surface receptors. *J. Biol. Chem.* 257:42–45.
7. Droz, B., H. J. Koenig, and L. di Giamberardino. 1973. Axonal migration of protein and glycoprotein to nerve endings. I. Radioautographic analysis of the renewal of protein in nerve endings of chicken ciliary ganglion after intracerebral injection of [^{3}H]lysine. *Brain Res.* 60:93–128.
8. Fertuck, H. C., and M. M. Salpeter. 1974. Sensitivity in electron microscope autoradiography for ^{125}I. *J. Histochem. Cytochem.* 22:80–87.
9. Forman, D. S., B. Grafstein, and B. S. McEwen. 1972. Rapid axonal transport of [^{3}H]fucosyl glycoproteins in the goldfish optic system. *Brain Res.* 48:327–342.
10. Grafstein, B., and D. S. Forman. 1980. Intracellular transport in neurons. *Physiol. Rev.* 60:1167–1283.
11. Griffin, J. W., D. L. Price, D. B. Drachman, and J. Morris. 1981. Incorporation of axonally transported glycoproteins into axolemma during regeneration. *J. Cell. Biol.* 88:205–214.
12. Harper, C. G., J. O. Gonatas, A. Stieber, and N. K. Gonatas. 1980. In vivo uptake of wheat germ agglutinin-horseradish peroxidase conjugates into neuronal GERL and lysosomes. *Brain Res.* 188: 465–472.
13. Hart, J. R. 1969. Some observations on the development of the avian optic tectum. Ph.D. thesis. The University of Wisconsin, Madison.
14. Hatten, M. E., and R. L. Sidman. 1977. Plant lectins detect age and region specific differences in cell surface carbohydrates and cell reassociation behavior of embryonic mouse cerebellar cells. *J. Supramol. Struct.* 7:267–275.
15. Hayes, B. P., and K. E. Webster. 1975. An electron microscope study of the retinoreceptive layers of the pigeon optic tectum. *J. Comp. Neurol.* 162:447–466.
16. Hendrickson, A. E., and W. M. Cowan. 1971. Changes in the rate of axoplasmic transport during postnatal development of the rabbit's optic nerve and tract. *Exp. Neurol.* 30:403–422.
17. Hughes, R. C. 1976. Membrane Glycoproteins. A Review of Structure and Function. Butterworths, Boston. 135–151.
18. Karlsson, J.-O. 1979. Proteins of axonal transport: interaction of rapidly transported proteins with lectin. *J. Neurochem.* 32:491–494.
19. Karlsson, J.-O., and J. Sjostrand. 1971. Rapid intracellular transport of fucose-containing glycoproteins in retinal ganglion cells. *J. Neurochem.* 18:2209–2216.
20. Karnovsky, M. J. 1971. Use of ferrocyanide-reduced osmium tetroxide in electron microscopy. *In* Eleventh Annual Meeting American Society for Cell Biology, New Orleans. 146. (Abstr.)
21. LaVail, J. H., and W. M. Cowan. 1971. The development of the chick optic tectum. I. Normal morphology and cytoarchitectonic development. *Brain Res.* 28:391–419.
22. LaVail, J. H., S. Rapisardi, and I. K. Sugino. 1980. Evidence against the smooth endoplasmic reticulum as a continuous channel for the retrograde axonal transport of horseradish peroxidase. *Brain Res.* 191:3–20.
23. Lentz, T. 1972. Distribution of leucine-^{3}H during axoplasmic transport within regenerating neurons as determined by electron-microscopic autoradiography. *J. Cell Biol.* 52:719–732.
24. Levin, B. E. 1977. Axonal transport of [^{3}H]fucosyl glycoproteins in noradrenergic neurons in the rat brain. *Brain Res.* 130:421–432.
25. Levine, J., and M. Willard. 1980. The composition and organization of axonally transported proteins in the retinal ganglion cells of the guinea pig. *Brain Res.* 194:137–154.
26. Levine, J., and M. Willard. 1981. Fodrin: axonally transported polypeptides associated with the internal periphery of many cells. *J. Cell Biol.* 90:631–643.
27. Lorenz, T., and M. Willard. 1978. Subcellular fractionation of intra-axonally transported polypeptides in the rabbit visual system. *Proc. Natl. Acad. Sci. U.S.A.* 75:505–509.
28. McLaughlin, B. J., J. G. Wood, and J. W. Gurd. 1980. The localization of lectin binding sites during photoreceptor synaptogenesis in the chick retina. *Brain Res.* 191:345–357.
29. Marchisio, P. C., F. Gremo, and J. Sjostrand. 1975. Axonal transport in embryonic neurons. The possibility of a proximo-distal axolemmal transfer of glycoproteins. *Brain Res.* 85:281–285.
30. Margolis, T. P., and J. H. LaVail. 1981. Rate of anterograde axonal transport of [^{125}I] wheat germ agglutinin from retina to optic tectum in the chick. *Brain Res.* 229:218–223.
31. Margolis, T. P., C. M.-F. Marchand, H. B. Kistler, Jr., and J. H. LaVail. 1981. Uptake and anterograde transport of wheat germ agglutinin from retina to optic tectum in the chick. *J. Cell Biol.* 89:152–156.
32. Mercurio, A. M., and E. Holtzman. 1982. Ultrastructural localization of glycolipid synthesis in rod cells of the isolated frog retina. *J. Neurocytol.* 11:295–322.
33. Palay, S. L., and V. Chan-Palay. 1974. Cerebellar Cortex Cytology and Organization. Springer-Verlag, New York.
34. Pfenninger, K. H., and M.-F. Maylié-Pfenninger. 1981. Lectin labeling of sprouting neurons. II. Relative movement and appearance of glycoconjugates during plasmalemma expansion. *J. Cell Biol.* 89:547–559.
35. Rager, G. H. 1980. Development of the retinotectal projection in the chicken. *Adv. Anat. Embryol. Cell Biol.* 63:1–92.
36. Repérant, J., and P. Angaut. 1977. The retinotectal projections in the pigeon. An experimental optical and electron microscope study. *Neuroscience.* 2:111–118.
37. Rosenbluth, J. 1962. Subsurface cisterns and their relationship to the neuronal plasma membrane. *J. Cell Biol.* 13:405–421.
38. Ruda, M. A., and J. D. Coulter. 1980. Lectins as markers for studies of axonal connectivity. *Soc. Neurosci. Abstr.* 6:339.
39. Sabatini, D. D., G. Kreibich, T. Morimoto, and M. Adesnik. 1982. Mechanisms for the incorporation of proteins in membranes and organelles. *J. Cell Biol.* 92:1–22.
40. Salpeter, M. M., and L. Bachman. 1972. Autoradiography. *In* Principles and Techniques of Electron Microscopy. Biological Applications. M. A. Hayat, editor. Van Nostrand Reinhold, New York. 2:221–278.
41. Salpeter, M. M., L. Bachman, and E. E. Salpeter. 1969. Resolution in electron microscopic autoradiography. *J. Cell Biol.* 41:1–20.
42. Salpeter, M. M., and M. G. Farquhar. 1981. High resolution analysis of the secretory pathway in mammotrophs of the rat anterior pituitary. *J. Cell Biol.* 91:240–246.
43. Salpeter, M. M., H. C. Fertuck, and E. E. Salpeter. 1977. Resolution in electron microscope autoradiography. III. Iodine-125, the effect of heavy metal staining, and a reassessment of critical parameters. *J. Cell Biol.* 72:161–173.
44. Salpeter, M. M., and F. A. McHenry. 1973. Electron microscope autoradiography. Analyses of autoradiograms. *In* Advanced Techniques in Biological Electron Microscopy. J. K. Koehler, editor. Springer-Verlag, New York. 113–152.
45. Salpeter, M. M., and M. Szabo. 1976. An improved Kodak emulsion for use in high resolution electron microscope autoradiography. *J. Histochem. Cytochem.* 24:1204–1209.
46. Schnapp, B. J., and T. S. Reese. 1982. Cytoplasmic structure in rapid-frozen axons. *J. Cell Biol.* 94:667–679.
47. Schonbach, J., C. Schonbach, and M. Cuénod. 1971. Rapid phase of axoplasmic flow and synaptic proteins: an electron microscopical autoradiographic study. *J. Comp. Neurol.* 141:485–498.
48. Schwab, M. E., K. Suda, and J. Thoenen. 1979. Selective retrograde transynaptic transfer of a protein, tetanus toxin, subsequent to its retrograde axonal transport. *J. Cell Biol.* 82:798–810.
49. Sharon, N., and H. Lis. 1975. Use of lectins for the study of membranes. *Methods Membr. Biol.* 3:147–200.
50. Siegel, S. 1956. Nonparametric Statistics for Behavioral Sciences. McGraw Hill, New York. 127–131.
51. Small, J. V. 1968. Measurement of section thickness. In Proceedings of Fourth European Regional Conference on Electron Microscopy. D. S. Bocclanelli, editor. Tipografia Poliglotta Vaticana, Roma. 1:609–619.
52. Tessler, A., L. Autilio-Gambetti, and P. Gambetti. 1980. Axonal growth during regeneration: a quantitative autoradiographic study. *J. Cell Biol.* 87:197–203.
53. Thompson, E. B., J. H. Schwartz, and E. R. Kandel. 1976. A radioautographic analysis in the light and electron microscope of identified *Aplysia* neurons and their processes after intrasomatic injection of L-[^{3}H]fucose. *Brain Res* 112:251–281.
54. Tytell, M., M. M. Black, J. A. Garner, and R. J. Lasek. 1981. Axonal transport: each major rate component reflects the movement of distinct macromolecular complexes. *Science (Wash. DC).* 214:179–181.
55. Weibel, E., G. Kistler, and W. Scherle. 1966. Practical stereological methods for morphometric cytology. *J. Cell Biol.* 30:23–38.
56. Willingham, M. C., and I. H. Pastan. 1982. Transit of epidermal growth factor through coated pits of the Golgi system. *J. Cell Biol.* 94:207–212.
57. Wood, J. G., F. I. Byrd, and J. W. Gurd. 1981. Lectin cytochemistry of carbohydrates on cell membranes of rat cerebellum. *J. Neurocytol.* 10:149–159.